


paper 5

 [Composite Structures 294 \(2022\) 115722](#)

Contents lists available at [ScienceDirect](#)

Composite Structures

journal homepage: www.elsevier.com/locate/compstruct

Design and construction of modern FRP Japanese bows by an inverse 
modelling approach of the elastica theory Giacomo Mariani a,*, Eiichi
Obataya b, Mahiro Kosaka c, Makinori Matsuo c

a Graduate School of Pure and Applied Sciences, University of Tsukuba, 1-1-1 Tennodai, 305-8571, Japan b Faculty of Life and Environmental Sciences, University of Tsukuba, 1-1-1 Tennodai, 305-8572, Japan c Faculty of Health and Sport Sciences, University of Tsukuba, 1-1-1 Tennodai, 305-8574, Japan

ARTICLE INFO

Keywords: Bow manufacturing Glass fibre Elastica theory Japanese archery

ABSTRACT

Modern archery bows employ composite limbs of organic materials and fibre-reinforced plastics (FRP) to increase strength and durability in a lightweight structure [Code a1]. However, empirical methods are often

employed for the manufacturing of the bows. [Code a2] We propose a systematic method for the design and fabrication of FRP bows based on an inverse modelling approach of the elastica theory, which significantly simplifies the analysis of the bow's limb deformation [Code a2]. The construction materials are analysed by the three-point bending test and by strain gauges. We manufacture three asymmetric FRP Japanese bows with a length of 1.6 m, a force of 5 kgf, and different unbraced curvatures by using wood and glass fibre laminates. [Code a3] The excellent matching between the manufactured bows and the design is confirmed by a small discrepancy in the measurements of bending stress ($RMSE < 8$ MPa), final force ($< 5\%$), and deformation ($RMSE < 2$ mm) of the bows. [Code a4] The inverse model demonstrates the use of FRP in bows traditionally manufactured with organic materials, by posing constraints to preserve their long-established shape. [Code a4] Compared to the try-and-cut approach, our method provides the sufficient requirements and failure criteria for the construction of a bow's limb, without involving complex numerical simulations. [Code a5]

1. Introduction

Modern archery bows are fabricated with fibre-reinforced plastics (FRP), synthetic composite materials that can sustain a large elastic deformation, improving strength and repeatability in the performance of the act of shooting. Bow-makers traditionally employ wood in self or laminated bows and biological materials such as horn and sinew in highly recurved composite bows which undergo large deformation [1– 3]. Bamboo is also widely employed for its ductile behaviour providing high allowed deformation before crushing. These materials are accompanied by an intrinsic variability of their physical properties and high sensitivity to the environmental conditions. For this reason, traditional bows constructed with organic materials have started to integrate FRP to obtain repeatable results and increase the durability of the bows. Nowadays, glass or carbon fibre laminates are commercially available for archery, which combined with a light wood core offer a cost-effective solution for higher performances. Despite the integration of FRP in traditional bows, the procedure of the

design and construction is often performed by time-consuming try-and-cut methods. Thus, a simple and practical modelling method of design which can benefit from the properties of FRP is required.

The modelling of the bows was introduced by Hickman, Nagler and Klopsteg [4,5] for the description of bows with symmetric limbs, by using analytical equations and simplified assumptions applicable to bows with a certain shape. Later, the design of symmetric bows and the analysis of the materials were treated by Kooi by means of a numerical resolution of the Euler–Bernoulli elastica theory [6–8]. More recently, 3D modelling and finite-element analysis (FEA) have given a further insight of the distribution of the material stress inside the bow [9– 11]. More general models for bows with asymmetric limbs were also developed [12–15]. On the one hand, the design of the bows treated in the previous studies aims to optimize the limb’s shape and material, to store a high elastic energy in a light structure and increase the propelling efficiency of the arrow. On the other hand, the shape of traditional bows is well established and a method for obtaining accurate results from their manufacturing is rather required.

For this purpose, here we propose a systematic method for the design of traditional bows built with FRP by using an inverse modelling approach of the elastica theory. Compared to Ref. [4–8], the model applies to any bow with symmetric or asymmetric limbs, for exception of the modern compound bow. In this method, we inversely

* Corresponding author.

E-mail address: mariani.giacomo.wp@alumni.tsukuba.ac.jp (G. Mariani).

<https://doi.org/10.1016/j.compstruct.2022.115722>

Received 7 December 2021; Received in revised form 12 April 2022;
Accepted 8 May 2022

Available online 13 May 2022



Fig.1. Commercial Japanese Hankyu bow in its braced condition and arrows (Photo credit to K. Sakamoto and C. Broggi).

use the full drawn profile of the bow as initial condition for the design and we derive the unbraced shape of the bow necessary for the construction, as opposed to Ref. [6,7]. This is an advantage for bows with established shapes over a numerical or practical trial and error procedure of optimization. By choosing a desired final force of the bow, the geometrical dimensions for the construction of the limb, such as width and thickness, are given by the sandwich theory [16]. From the referred to as “target”. Based on the existing FRP Japanese bows, we determine a target profile to use for this study, as shown in Fig. 2a. To derive the inverse equation we start from the elastica equation in curvilinear coordinates, derived by Kooi [20] for the study of symmetric bows and used in Refs. [15] for the study of bows with asymmetric limbs: $d^2\theta/ds^2 = M(s)/K_I h(s)$, $\theta = \theta(s) - \theta(0)$, (1)

geometry of the limb, the calculation of the maximum stress allows to ds_i

$$W(s_i)$$

$$W(s_i)$$

$$i \ i$$

$$0 \ i$$

evaluate potential failures and determines the choice of the suitable materials to assemble the bow. Our simplified model provides the sufficient conditions for the manufacturing of the bow, without using the complex analytical or numerical methods used in Ref. [12–15], and without entering in detail of the bow dynamics.

We apply the inverse model for the design and construction of the modern FRP Japanese bow, which constitutes the general case of asymmetric bow with large deformation. In Japanese archery, FRP laminations were introduced in the late 60s by Miyata [17,18] and Koyama [19], following the fame of the western bows. The Japanese FRP bow, initially adopted as a convenient and cheap solution for beginners, when compared to delicate traditional bamboo bow, was gradually accepted and became essential in the archery community. The shape of the bow slightly changed to adapt to the FRP materials but the characteristic asymmetric shape was preserved to maintain the long-established tradition. To validate our model, we decide to construct the Japanese Hankyū (lit. “half bow”), a short Japanese bow, as shown in Fig. 1. This bow has a length of ~ 1.6 m and typical drawing forces in a range of 4–6 kgf. We choose this particular bow, as compared to the longer bow (~ 2.2 m) used in Kyūdō (Japanese archery), for its easier construction and lower drawing force which allows us to study its properties more extensively. We construct three bows made of glass fibre and wood laminates, with different initial curvature and same final force of 5 kgf, showing that at full draw all the bows converge to the same deformed shape set by the model. To complete the characterization of the bows and validate the inverse model, we use the direct numerical resolution of the elastica equations described in Ref. [15].

This manuscript is organized as follows. In Section 2 we derive the inverse equations and we present the systematic method to derive the dimensions and shape of the bows used for their construction. In Section 3 we measure the properties of the materials and we analyse their criteria of selection, based on the calculation of the bending stress and springback effect. In Section 4 we discuss the characteristics of the constructed bows and we describe our experimental setup. Then, we compare the experimental data

of force, deformation, and stress with the results of the inverse model. In Section 5 we summarize our conclusions and final remarks.

1. Inverse model and design of the bow

where $M(s) = Kh(s)$ is the bending moment, $K = \frac{1}{R}$ is the absolute value of the string tension, $W(s_i)$ is the bending stiffness of the limbs, and θ_i , $\theta_0(s_i)$ are the final and initial angles formed by the limbs with respect to the y -axis, respectively. The distance h is given by $h(s_i) = b - x(s_i) \cos \theta_i - y(s_i) \sin \theta_i$, (2)

[]

where $x(s_i)$ and $y(s_i)$ are the final coordinates of the bow, θ_i is the angle formed by the string with respect of the y -axis, and b is the draw length of the bow. The quantities with pedix 0 refer to the unbraced shape of the bow. The quantities related to the upper and lower limbs are explicitly indicated by the pedix $i = U$ (up), D (down), respectively, or written as a function of the curvilinear coordinate s_i of the limb's length. The grip of the bow is located at $s_i = 0$, the starting point of the upper and lower limb. For more details we refer the reader to Ref. [20] for the derivation of Eqs. (1) and (2). By numerically solving the previous equations, the static characteristics of the bow can be determined. The direct numerical resolution is described in Ref. [15] and is hereinafter referred to as “direct model”. In Eq. (1) we neglect the shear deformation of the bow, considering the typical lengths of the Japanese bows in a range of 1.6–2.2 m, large as compared to the thicknesses of the limbs in a range of 7–15 mm. Assuming a thin limb, we model the profile of the bow using the line of curvature correspondent to belly side of the bow.

From the condition of static equilibrium $K_U \cos \theta_U = K_D \cos \theta_D$ along the y -axis, we can explicitly write Eq.(1) as a function of the target force of the bow at full drawn $F = \frac{1}{b} (b) = K \sin \theta + K \sin \theta$.

|| $b U U D D$

We define a constant of proportionality k as []

$k = \tan \varphi_U + \tan \varphi_D^{-1}$, (3) and from the bending moment $M(s_i)$ we define a reduced function of the bending moment: $m(s_i) = b - x(s_i) - y(s_i) \tan \varphi_i$

. (4) In Eq. (1), taking a monotonic distribution of the stiffness we rewrite $W(s_i) = W_{max} w(s_i)$, where $W_{max} = W(s_i = 0)$ is the maximum bending stiffness taken at $s_i = 0$ and $w(s_i)$ is the normalized stiffness distribution.

Substituting the previous quantities in Eq.(1), we can write the inverse elastica equation in the integral form for the angle of the unbraced bow as

$$\varphi(s) = \varphi(0) - k(Fb) \int_0^s m(s_i) ds. \quad (5)$$

i

i

W_{max}

\int_0

$w(s_i)$

i

The coordinates of the unbraced bow can be calculated as:

The design of the unbraced shape of the bow necessary for the construction starts from a profile of the bow fully drawn, hereinafter

$$x_0(s_i) = \int$$

0

s_i

$$\sin \int_0^{s_i} \varphi_0(s_i) ds_i, y_0(s_i) = \int$$

0

s_i

$$\cos \int_0^{s_i} \varphi_0(s_i) ds_i \cdot (6)$$



Fig. 2. (a) Target profile of the bow (black line) used as initial condition for the design. (b) Unbraced shapes (black lines) of the bows computed as a function of r by using the inverse model with $w_m = 0.4$. The grey line for $r = 1.1 \text{ m}^{-2}$ represents the limit for which the shape of the unbraced bow converges to its braced situation. The inset shows the relation between the ratio r and the *urazori*, the reflex height u of the bows. (c) Normalized stiffness distribution $w(s_i)$ chosen for the designed bows. (d) Force curves for the bows shown in (b) computed by using the direct model [15].

Eqs.(5)and(6)can be solved numerically by using e.g. the trapezoidal rule. Eq. (5) is calculated as a function of the target coordinates and as a function of the force-to-maximum stiffness ratio $r = F_b / W_{max} \cdot F_b$

total string length of $sl_{tot} = sl_U + sl_D = 0.978 \text{ m} + 0.602 \text{ m} = 1.580 \text{ m}$. For low values of r , the shape of the unbraced bow reaches a limit as it converges to its braced shape when

is expressed in unit of Newton (N), whereas in the text we refer to kilogram-force (kgf), the typical unit used in archery. From Eqs. (5) *sltot*

$$= \sqrt{[y(L_U$$

$$) - y(L_D$$

$$)]^2 + [x(L_U$$

$$) - x(L_D$$

$$)]^2, (8)$$

and(6)we can derive the profile of the unbraced bow that is used for the manufacturing. For simplicity, we assume that the string is contact with the bow only at the end of the limb or that the part in contact with the bow is short. As shown inFig.2b, we study the unbraced shape of the bow as a function of r , where a higher r corresponds to a more pronounced recurve of the unbraced bow. We generate the curves by using a fixed linear distribution of the bending stiffness, as shown in Fig. 2c. The inset ofFig. 2b shows the height of the bow or *urazori*, which is used in Japanese archery to evaluate the amount of the bow's recurve. The profile of the target shown in Fig. 2a is given by $x(y) = 10.5695y^{10} - 26.5203y^9 + 17.0983y^8 + 10.3205y^7$


$$-17.3688y^6 + 2.9292y^5 + 4.6760y^4 - 1.4348y^3$$

$+0.2770y^2 - 0.1920y$, (7) with $-0.510 \text{ m} \leq y \leq 0.907 \text{ m}$, $b = 0.65 \text{ m}$, and the string angles $\angle_U = 32.08^\circ$, $\angle_D = 21.98^\circ$. The Cartesian coordinates are then transformed in curvilinear coordinates taking $x(s_i=0) = y(s_i=0) = 0$. The

total length of the bow is $L_{tot} = L_U + L_D = 1.00 \text{ m} + 0.62 \text{ m} = 1.62 \text{ m}$, with
a
for $r \sim 1.1 \text{ m}^{-2}$, as shown in Fig. 2b. As shown in Fig. 2d, for $r \sim$

1.1 m^{-2} the curve is tangent to $F_b = 0$, thus the string has no tension in its braced condition ($K_i = 0$), for which the bow loses its propelling power. The curve for $r < 1.1 \text{ m}^{-2}$ indicates that with the constraint of the string length sl_{tot} imposed by the target, the string is not naturally in tension until $b \sim 0.25 \text{ m}$. For lower b , the bow would require negative forces to maintain this tension, which is not physically applicable. As r increases, the energy stored in the bows represented by the area below the curves, increases. For $r = 3.5 \text{ m}^{-2}$ and 4.0 m^{-2} the bows are unstable for the case of $w_m = 0.4$ and for low b we did not obtain accurate solutions. Further results of the direct model and other approaches of the inverse model are discussed in Supp. Mat.

To experimentally demonstrate the inverse model, we fabricate three Hankyu[−] bows with curvatures corresponding to $r = 1.5, 2.0$, and 2.5 m^{-2} , as shown in Fig. 2b. We refer to these samples as H1.5, H2.0, and H2.5, respectively. We choose to fabricate all the three bows with the same final force of $F_b = 5 \text{ kgf}$, reached at the full drawn profile of the target for $b = 0.65 \text{ m}$. To confirm the inverse model's validity and complete the bows' characterization, the variation of the

 limb is highly deflected, we take the centroid and the neutral axis as coincident at the centre of the cross-section as in the case of a straight beam (see Supp. Mat). The stiffness of the sandwich beam is given by $12 + E_t 6 + E_t$

(12)

$l [$

$$W(s_i) = a(s_i) E_c$$

$$c(s_i)^3$$

$$t^3$$

$$t(c(s_i) + t)^2]$$

$$2$$

Fig. 3. Sandwich structure of the limb's cross-section before (a) and after (b) the assembly of the bow. In (a) the materials are pre-stressed and we consider p , the pressure, where E_c, E_t are the Young moduli of the materials of core and faces, respectively, which are measured by the three-point bending test shown in Section 3. We construct the bows with a variable thickness and width of the limbs along their length. Excluding the string stoppers, the limbs have a total thickness of $d = c + 2t$, with $c = c(s_i)$ the variable thickness of the core and t the constant thickness of the faces. For the construction of the bows, we use glass fibre laminates with a constant thickness of $t \sim 1$ mm. The limb of the long Japanese bow is narrower and thicker as compared to the western bows. To maintain the same proportions in the shorter Hankyu, we first constrain the width of the limb $a(s_i)$

distance from the centroid to the surface of the single elements. In (b) we evaluate

to a maximum of $A = 24$ mm at the grip, linearly decreasing to a

max

the stress of the materials considering q , the distance from the centroid of the whole structure.

minimum of A

min

= 20 mm at the limb's ends as

$$a(s) = A [(1 - a) \cdot (Li - si) + a], 0 \leq s \leq L, (13)$$

quantities concerning the draw length
is calculated by using the direct
 $i max m$

$Li m$

$i i$

b

model [15].

with $a_m = A_{min}/A_{max}$. The shape of the limb is linked to the character-In

the following sections, we design the cross-section of the bow's limb by using a non-curved or straight beam approximation. We approximate an average radius of curvature R across the cross-section, considering the limb thin compared to R . With this approximation, we commit an error of less than 5% if $R/d > 10$ for the calculation of the stress [21], where d is the total thickness of the beam. In the case of the Hankyu bow, $R_{max}/d \sim 0.33/0.007 = 47$, but this is also true for the longer Japanese bow where $R_{max}/d \sim 0.50/0.015 = 33$. This approximation is further discussed in Supp. Mat.

2.2. Bending stiffness and limb's geometry A monotonic distribution of the stiffness decreasing from the grip of the bow to the limb's ends is left as a free parameter to set. In this work, for the bow's limbs we choose a linear distribution of the stiffness $w^l(s_i)$. To complete the analysis, we consider the string stoppers at limb's ends which are covered with an additional layer of wood. Introducing the additional distribution of the string stoppers $w^{st}(s_i)$, the total stiffness distribution is given by $w(s) = w^l(s) + w^{st}(s)$, (9)

istic technique of Japanese archery, which requires a narrow limb for the hand to wrap around the grip and to facilitate the rotation of bow around its centroid at the arrow's release.

At this point, the thickness of the limb d is calculated to produce the required force of the bow. The curvature of the bow is fixed by the ratio r and by the stiffness distribution of Eq. (9) inserted in Eq. (5). The final force of the bow is fixed by F_b . The required maximum stiffness for the manufacturing of the bow is $W_{max} = F_b/r$. Then, by using Eqs. (10), (12) and (13), the thickness distribution of the core $c(s_i)$ is numerically computed finding the root of

$[W_{max}w^l(s_i) - W^l(c(s_i))] = 0$ (14) with respect of $c(s_i)$. To compute the thickness of the string stoppers at the limb's ends, the bending stiffness $W^{st}(s_i)$ for a four-layered beam is used (see Supp. Mat.). The thickness $e(s_i)$

of the string stoppers is numerically computed, finding the root of $[W_{max}w(s_i) - Wst(e(s_i))] = 0$ with respect of $e(s_i)$. The results of the design and the comparison with the manufactured bows are reported in Supp. Mat. The string stoppers are short when compared to the length of the bow and the bending moment toward the limb's ends approaches zero. Thus, the

$i i i$

with

additional stiffness from the string stoppers at the end of the limb does not affect the bow's static properties and it may be neglected with good

$$w^l(s) = (1 - w) \cdot (Li - si) + w$$

i

m

L_i

m

i

i

is calculated as

, $0 \leq s \leq L$, (10)
approximation. To complete the analysis, the total weight of the bow

$()_2$

$) = [1 -$

)]

$$s_i-Lst$$

$$w^{st}(s_i$$

$$w^l(s_i$$

.

i

$$,s_i$$

$$\geq$$

$$P \simeq \sum \sum \square S\left(s\right) \mathrm{d} s\;, \left(15\right)$$

$$Li$$

$$n\int$$

$$n$$

i

i

i

$$n$$

$$0$$

$$L_i - L_{st} \quad i$$

i

$$L_{st} ,$$

where ρ_n and S_n are the density and cross-sectional area of the n -part,

with $w_{st}(s_i) = 0$ for $s_i < L_{st}$. In Eq. (10), $w_m = W_{min}/W_{max} > 0$ is the (11)

respectively. For simplicity, the adhesive is neglected in the calculations

normalized stiffness at the limb's ends and in Eq. (11), L_{st} is the starting i

of the stiffness since its Young modulus $E_a \sim 1$ GPa and thickness are

points of the stoppers, as shown in Fig. 2c. We set $L_{st} = 0.90$ m and $L_{st} = 0.55$ m. It should be noted that for a chosen force $^U F$, a reduction b

negligible when compared to the other elements. However, we expect the real weight of the bow to be higher than that calculated in Eq. (15).

of $^D w$ influences the shape of the unbraced and braced bow adding m

more recurve to the final part of the limbs. Excessively small values of w_m lead to unstable bows in practice [20]. To obtain a braced shape similar to the existing Japanese bows we set $w_m = 0.4$, as shown in Fig. 2c. From Eq. (5), for a fixed ratio r which determines the amount of recurve of the bow, the final force of the bow varies linearly as a function of the maximum

stiffness as $F_b = r \cdot W_{max}$. In the design of the bow once the desired F_b is set, the dimensions of limbs are derived from the correspondent W_{max} .

For the design of the limb's cross-section, we use a rectangular sandwich beam [16] in which a light wood core is interposed between two stiff glass fibre layers, as shown in Fig. 3. Although the bow's

1.

Characterization of the materials and stress of the bow

To calculate the dimensions of the limbs, we conduct a quantitative analysis of the mechanical properties of the materials that we use for the fabrication of the bows: glass fibre and wood.

3.1. Bending test

We measured the properties of a commercial unidirectional (UD) (0°) glass fibre laminate for archery with a rated 75% fibre weight content and seven different wood species, by using the three-point

Table 1

Glass fibre and woods tested by using the three-point bending test. The measured woods have a moisture content (MC) < 15% determined from the oven dry weight of the specimens. The reported values are calculated as an average of three or more specimens.

Material	E (GPa)	MOR (MPa)	σ_{el} (MPa)	ρ (kg/m ³)
GFRP (UD)	~37	>600	~400	~1750
Spruce	7.1	48.8	35.8	330

Jap. cedar	8.6	58.7	44.7	358
------------	-----	------	------	-----

Jap. cypress	11.7	86.7	62.3	410
--------------	------	------	------	-----

Lauan	10.7	92.3	65.8	461
-------	------	------	------	-----

Jap. red pine 13.0 100.4 74.3 488

Beech 12.1 125.4 75.2 704

Cherry tree 12.2 133.5 75.6 717

bending test, as shown in Fig. 4. The woods were provided by a local lumber shop. The measurements were performed in a conditioned room at a temperature of 20°C and relative humidity of 60%. We measured four softwoods: spruce (*Picea*), Japanese cedar (*Cryptomeria japonica*), cypress (*Chamaecyparis obtusa*), red pine (*Pinus densiflora*), and lauan (*Shorea*). Then, we measured two hardwoods: beech (*Fagus*) and cherry (*Prunus serrulata*). The properties of the measured materials, Young modulus, the elastic limit of the materials σ_{el} , modulus of rupture (MOR), and density are summarized in Table 1. Glass fibre shows a Young modulus of ~ 37 GPa, much larger than the one of the woods in a range of 7–13 GPa, and a high elasticity up to a large deformation of $\sim 1\%$. The glass fibre used in a sandwich structure makes the limb heavier but thinner compared to the only wood, reducing the stress in the core and making the total stiffness less sensitive to the material of the core. The suitable wood for the core of the limb is the lightest that can be elastically deformed without breaking.

The maximum bending stress which occurs in the target profile of the bow is given as a superposition of σ_{pre} , the pre-stress of the laminates before the assembly, and σ_{bow} , the stress induced by the deformation of the limb after the assembly, assuming a thin beam and the elastic deformation of the materials. The general formula of the stress $\sigma = (EMy)/W$ can be rewritten from Eq. (5) as



Fig. 4. Three-point bending test of a thin glass fibre laminate and various wood specimens. (a) Glass fibre and (b) Japanese cypress chosen for the

construction of the bows. The inset shows the wood specimen under test.
 (c), (d) Other softwoods and hardwoods tested for a comparison.

$$\Delta = \Delta$$

$$+ \Delta$$

$$= E$$

$$\cdot$$

$$k \cdot r \, m(s_i) \, q \, (s \,)$$

$$_{tot}$$

$$_{bow}$$


$$_{pre \, n}$$

$$w(s_i)^{n \, i}$$

$$+E_n \, \Delta_0(s_i) - \Delta_{pre}(s_i) \, p_n(s_i) \, , \, (16) \, [\,]$$

where the pedix $n = c, t$ indicates the outermost fibres of the n th element of the cross section, core or faces of the sandwich limb, with E_n the Young modulus. As shown in Fig. 3, q_n is the distance from the centroid of the

cross-section, whereas p_n is the distance from the centroid of the n th element. These quantities can be calculated from

 Fig. 5. Weight of the bows calculated by using Eq. (15) for different final forces and curvatures by using the values of glass fibre and Japanese cypress in Table 1.

weight of the bow given by Eq. (15) rewritten as 1

3

the thickness distribution of the limb derived from Eq. (14). We define $P = \sum$

$$\frac{1}{12} (F_b)^3$$

$$Li [w(s) a(s)^2] ds, \quad (18)$$

the curvature of the unbraced bow as $\kappa_0(s_i) = d\kappa_0(s_i)/ds_i = 1/R_0(s_i)$ and $i=U, D, E, 1/3, r, \int_0$

i i i

the initial curvature of the laminates before the assembly as κ_{pre} . In the case of a self-bow directly constructed from a single piece of wood, we

have $\sigma_0 = \sigma_{pre}$ and thus there is no pre-stress in the material. In our case, since we initially use straight laminates, we can assume $\sigma_{pre} = 0$.

Before evaluating Eq. (16) to identify a suitable wood core for the sandwich limb, we first consider the simple case of a rectangular limb of thickness d , width a , cross-sectional area $S = d \cdot a$, and Young modulus E , made of a single material with negligible pre-stress. At the grip of the bow for $s_i = 0$, where the maximum stress usually occurs, we have $m(0) = b$ and the thickness is given by $d(0) = [12W(0)Ea(0)]^{1/3}$ with $q(0) = d(0)^2$ and $W(0) = W_{max} = F_b/r$. Substituting the previous relations in Eq.(16), the first condition for the construction of an elastic bow is (3)

where the ratio $\sigma_0^{1/3}$ should be minimized for the lightest bow. Eqs. (17) and (18) also tell that for a fixed force F_b , a higher curvature of the bow given by r , gives lighter limbs but higher stress in the material.

The same procedure applies to the sandwich beam where this time the thickness of the core $C(s_i)$ is derived as shown in Section 2.2. The total weight calculated using the values of glass fibre and Japanese cypress of Table 1 in Eq. (15) is shown in Fig. 5. The weight predicted for the H1.5, H2.0, and H2.5 bows is around 0.2 kg. As expected by Eq.(18), the weight decreases by increasing the curvature of the bow, whereas for a fixed r the weight increases by increasing the force of the bow.

3.2. Stress simulation

□□□

$E^{3/2}$

$> k$

$$F_b$$

$$2 a(0)$$

$$^3 b \cdot r^{23}, (17)$$

Based on the properties measured by the three-point bending test,

where the ratio $\sigma_{el}/E^{3/2}$ should be maximized. Among the materials which satisfy this condition, the lightest is chosen by minimizing the weight. We calculated the thickness distribution and stress of the bows for different woods. For the construction of the bows we chose the Japanese



Fig. 6. Simulations of the absolute value of the maximum stresses recorded on the limbs as a function of the final strength F_b and curvature represented by the r . The stress is evaluated at the outermost fibres of each material. The total stress is evaluated for the target profile of the bow, full drawn at $b = 0.65$ m. (a) Pre-stress of the wood core as a function of the number of layers N . (b) Pre-stress of the glass fibre. (c) Total stress of glass fibre. (d) Total stress of the wood core as a function of the number of layers $N = 1, 2, 3$ in which is divided. (e) Stress of the bow on the wood core, which corresponds to a large N . Simulations are performed by using $E_f = 37$ GPa and $t = 1$ mm and the value of Japanese cypress in Table 1. The black points indicate the position of the H1.5, H2.0 and H2.5 bows. The dashed lines indicate the limit of the elastic stress σ_{el} . The red line indicates the maximum allowed stress (MOR).

cypress as the core of the limb for its low density and sufficiently high elastic stress. In choosing the material, we consider two failure mechanisms in the bow, given by Eq.(16). The first one, which occurs during the bow's construction, is the pre-stress σ_{pre} of the laminates which exceeds the maximum allowed stress of the materials when bent on the mould. A laminated limb is constructed by bonding and bending together several layers on a mould with the shape of the bow. The hardening of the adhesive maintains the shape, and thus a pre-stress in the single layers remains. The second one, which occurs during the maximum deformation of the finished limb, is the total stress of the target σ_{tot} which exceeds the maximum allowed stress or MOR. σ_{tot} is evaluated at $b = 0.65$ m, when the bow is fully drawn.

By using Eq. (16), the results of the numerical simulation for a bow The results shown in Fig. 6c and e are consistent with Eq. (17), since for a negligible pre-stress the stress of the bow increases by increasing the force or the curvature of the bow.

3.3. Springback effect

The final aspect to consider for the choice of the most appropriate structure of the limb is the springback effect. The springback effect determines a loss of the curvature of a bonded laminated beam after curing in a mould [22]. This effect is caused by the sum of all the residual pre-stresses of the single layers, which produces an elastic bending moment that tends to restore the original shape of the layers. Considering a thin limb, the variation in the curvature due to the springback effect is given by

constructed with Japanese cypress and glass fibre are shown in Fig. 6,
 $d\kappa_0$

$d\kappa_{sp}$

M_{tot}

where the absolute value of the maximum stress at the outermost fibres (compression or tension) of the layers is evaluated. The maximum pre-stress –

$$ds = R_0 - R$$

sp

$$= W$$

$_{tot}$

, (19)

stress in the core calculated for $p_c = c(2 \cdot N)$, can be linearly reduced by dividing the core in N layers of the same material, as shown in Fig. 6a. We assume that the division in multiple layers does not affect the stiffness. In the case of the H1.5, H2.0, and H2.5 bows with a force of 5 kgf, the wood core's pre-stress is always within the elastic limit. In the case of glass fibre, the laminates are thin enough so that the maximum pre-stress evaluated at $p_t = t/2$ is negligible when compared

where α_0 and α_{sp} are the angles of the designed bow and springbacked bow after the adhesive has cured and R_0 , R_{sp} the respective radius of curvature. W_{tot} is the total stiffness of the bonded sandwich beam. In the regime of elastic deformation of the materials, M_{tot} is the sum of the bending

moments of the single n layers of the limb given by $M_{tot} = \sum M_n \approx 1 \sum W_n \cdot (20) R_0$

n

n

to the maximum stress allowed, as shown in Fig. 6b. Furthermore, the maximum total stress of glass fibre evaluated at $q_t = c/2 + t$, is well below the elastic limit in a wider range of forces F_b and curvatures r of the bow, as shown in Fig. 6c. Fig. 6d shows the effect of $N = 1, 2, 3$ divisions of the core on the maximum total stress of the wood evaluated at $q_c = c/2$. For $N = 1$, the H1.5 and H2.0 bows exceed the elastic limit σ_{el} whereas, for $N = 2$, all the bows are below σ_{el} . For $N = 3$, the stress is further reduced and more uniform in the three cases. In the extreme case of a large number of thin layers ($N \rightarrow \infty$), where W_n is the bending stiffness of the single layers, and R_0 the single averaged radius of curvature for all the layers.

In a simple case, we consider a rectangular cross-section of thickness d and width a , of a single material with Young modulus E and total stiffness $W_{tot} = Ead^3/12$, composed by n layers with thickness d/n bent in a radius of curvature R_0 . Then, the single layers exert a total bending moment $M_{tot} = n \cdot M_n = Ead^3/(12R_0n^2)$. Substituting these quantities in Eq. (19), we obtain a normalized curvature variation of $\sigma_0 - \sigma_{bow} = 1$, (21)

the pre-stress is suppressed for which $\sigma_{tot} = \sigma_{bow}$, as shown in Fig. 6e.

σ_0

n_2

Table 2

Summary of the characteristics of the constructed bows. From the left, type of bow for $r = 1.5, 2.0, 2.5 \text{ m}^{-2}$, measured force at $b = 0.65 \text{ m}$, Young modulus and thickness of the glass fibre laminates, Young modulus and density of the wood used in the core and for the string stoppers, weight of the finished and designed bows.

three laminates of Japanese cypress as a core and two laminates of glass fibre as skins with a constant width of about 30 mm. For each bow we measured the properties of the materials, as shown in Table 2. Since the core has a variable thickness as calculated in Section 2.2, for

Bow Force

$E_t t$

E_c

ρ_c

Weight

Weight

simplicity we planed the two outer layers with a constant thickness and

(kgf) (GPa) (mm) (GPa) (kg/m³) Exp. (g) Des. (g) H1.5 4.92 37.4 1.026
12.0 429 228 200

H2.0 5.04 37.2 1.025 11.2 429 221 188

H2.5 4.78 36.8 1.027 10.7 463 209 185



Fig. 7. (a) Schematic of the experimental setup for the static measurements of the bow. The black squares indicate the position of the strain gauges applied on the bows.

(b) A strain gauge applied on the surface of the glass fibre. (c) Lateral view of a limb of one of the constructed bows with a three-layered wooden core of Japanese cypress.

where $\kappa_0 = 1/R_0$ is the curvature. Eq. (21) tells that the springback

,*sp* ,*sp*

the third one in the centre with a variable thickness. The wood and glass fibre surfaces are sanded with 100 grid paper and gently wiped with acetone. For the bonding of the laminates, we use a commercially available epoxy adhesive, the Smooth-On EA-40 [23], evenly applied on all the surfaces. The layers are placed one by one on the mould and secured by using clamps positioned at a step of 5 cm along the limb. A rope wound around the mould further secures the layers' position to avoid the layers' lateral sliding. The mould is then placed in a home-made temperature-stabilized oven and cured for 6 h at an average temperature of 65 °C. At the end of the curing, the mould is allowed to cool down to room temperature. The raw bows are removed from the mould and the string stoppers are applied at the limb's ends. Then the bows are laterally planed to create the width distribution of the limb, from 24 mm at the grip to 20 mm at the

limb's ends. The lateral view of one of the finished bows is shown in Fig. 7c. For further details, the comparison between the measured and designed distribution of the thickness and width of the bows are shown in Supp. Mat. A picture of the three finished bows is shown in Fig. 8.

The shape, force, and stress of the constructed bows are accurately characterized by using a home-made drawing board, as schematically shown in Fig. 7a. The measurements are performed by using an Arduino Nano microcontroller and the HX711, a 24-bit programmable gain amplifier (PGA) (Avia Semiconductor, SparkFun breakout board module). The HX711 is set to a sample rate of 80 Hz and is used to acquire both force and strain of the bows. The force is measured by a calibrated load cell LC1205-K050 (A&D Co., Ltd.) used in compression; the overall resolution is around 0.01 kgf. The strain is measured by using strain gauges FLAB-6-11-3LJC-F (Tokyo Measuring Instruments Laboratory Co., Ltd) in a quarter bridge circuit. We applied 12 strain gauges on the surface of the glass fibre laminate on the back side of each finished bow at a step of 0.13 m to measure the stress distribution σ_{bow} of the bows, as shown in Fig. 7a, b. The pre-stress σ_{pre} , which depends only on the change in curvature and thickness of the single

effect can be rapidly suppressed by increasing the number of layers. In a sandwich beam where stiff FRP layers are used to increase the total stiffness, the springback effect is further reduced. The springback of laminates, is measured by using a strain gauge bonded on a straight glass fibre laminate which is then clamped along the mould of the bow. The bonding areas are prepared by sanding the surface with 400 grid

the sandwich beam can be evaluated by using W as of Eq. (12) and The displacement of the bows is measured by an optoelectric rotary paper and gently wiped with acetone. The strain gauges are bonded

$$\Sigma = () [$$

$$N$$

$$n Wn$$

$$a s_i$$

$$E_C 12 i^2$$

, where the core is divided in N

$$c(s)^3 +$$

$$t_3]$$

$$tot$$

layers.

with a cyanoacrylate adhesive at the limb’s centre, as shown in Fig. 7b.

We evaluated the springback effect along the limb of the H1.5, H2.0, and H2.5 bows as $100\% \cdot (\varphi_0 - \varphi_{sp}) / \varphi_0$. For a sandwich limb, the springback is in a range of 10%–20% for $N = 1$, 4%–5% for $N = 2$, and below 3% for $N = 3$.

$$E_t 6$$

1. Bow construction, results, and discussion

In this section, we describe the procedure for the fabrication of three Hankyu[™] bows named H1.5, H2.0, and H2.5 and the experimental results comparing the shape, force, and stress of the constructed bows with the simulation. We fabricated all the bows with a force of $F_b = 5$ kgf at a

full draw length of $b = 0.65$ m. Based on the results of the simulations, for the manufacturing of the bows we chose a three-layered wood core to reduce both the pre-stress and springback effect.

4.1. Experimental setup

To create the shape of the unbraced bows, we first fabricated three moulds with a profile calculated in Fig. 2b for $r = 1.5, 2.0$, and 2.5 m^{-2} by the inverse equation. Then, for each bow we prepared an encoder connected to the Arduino Nano for a resolution of ~ 0.5 mm. All the measurements are performed drawing the bows with a b from 0.15 m to 0.65 m with a drawing speed of 5 mm/s. The shapes of the bows are documented by marking their profile on a grid paper and recording the (x, y) coordinates of discrete points at a step of 5 cm along the limb with a resolution of 1 mm. The profile marked on the grid paper is the line of curvature of the belly side of the bows, which is also used for the simulations with the inverse model. The bows were strung by using a string with a total length of $sl_{tot} = 1.582$ m, calculated from the target profile and keeping the drawing point of the string to match the upper portion of the string at $sl_U = 0.978$ m and lower portion at $sl_D = 0.602$ m. For all the measurements, we used a home-built string composed of Dyneema fibres (SK99) to ensure a negligible stretching for precise results. Table 2 summarizes the measured force and weight of the finished bows.

We compared the force, the shape, and stress distribution of the constructed bows with that set by the target and by the inverse equations. Additional comparisons of the experimental results from a variation of the drawing length of the bows, are performed with the direct model of Ref. [15].



Fig.8. Picture of the three constructed Hankyu bows in their unbraced condition. From the top to bottom H1.5, H2.0, and H2.5 (Photo credit to K. Sakamoto).

4.2. Shape measurements

We first compare the profile of the finished bows with the shapes calculated from the inverse model corresponding to $r = 1.5, 2.0, 2.5 \text{ m}^{-2}$, as shown in Fig. 9a. The fabricated bows after removing them from the mould are in good agreement with the design. We obtained a low Root Mean Square Error (RMSE) between the measured points and the design, calculated as 1.0 mm, 1.9 mm, and 0.6 mm for the H1.5, H2.0, and H2.5 bows, respectively. We did not observe significant springback of the bows, showing the effectiveness of the three-layered wood core used in the limbs. We strung the bows with the string length set by the target profile and we measured a brace height of 0.126 m, 0.130 m, and 0.132 cm for the H1.5, H2.0, and H2.5 bows, respectively, which we confirmed by using the direct model.

We fully drew the constructed bows at a displacement of $b = 0.65 \text{ m}$ and we compared their deformation with the target profile set by Eq. (7), as shown in Fig. 9b. We obtained an excellent matching for all the bows with an RMSE between the measured and target profiles calculated as 1.2 mm, 1.9 mm, and 1.7 mm for the H1.5, H2.0, and H2.5 bows, respectively. It should be noted that as expected by the inverse model, the shape of all the bows fabricated with different initial curvatures and stiffness, converges to the same full drawn shape of the target. A further agreement of the deformation of the constructed bows with the elastica theory is demonstrated by comparing the direct model for the different displacements of the bows. The difference with respect to the model described in Ref. [15] is that the bow in the braced condition is computed by matching the string length to that of

Fig. 9. Comparison between the shapes of the constructed (red dot) and simulated (black line) bows. The data are recorded at step of 5 cm along the limb, from the line of the belly side of the bows marked on a grid paper. (a) Unbraced shapes of the bows after removal from the mould. (b) Target profile of the inverse model for $b = 0.65 \text{ m}$. The grey lines represent the string during the drawing.



Fig. 10. Comparison between the measured force curves (black squares) of the constructed bows at a step of ~ 0.5 mm and the normalized simulations computed by using the direct model.

the target profile, instead of prescribing the brace height, which is not known a priori. The results and procedures are described in Supp. Mat.

4.3. Force measurements

The force curves of the constructed bows, measured by using the drawing board, are shown in Fig. 10. The target force of the bows set by design at $F_b = 5$ kgf was closely matched by the constructed bows for which we obtained final forces of 4.92 kgf, 5.04 kgf, and 4.78 kgf for the H1.5, H2.0, and H2.5 bows, respectively. The final forces of the bows are in a good agreement with the design, showing the usefulness of the inverse model for the manufacturing of the bows. The discrepancy in the absolute value of the final forces is within the 5% and is attributed to the variability in the Young moduli of the laminates along the length of the limb and to small geometrical imperfections originated during the fabrication. To confirm this assumption, we compared the measured force curves with that predicted by the direct model. As shown in Fig. 10, the simulation, normalized with the measured final force of the bows, shows an excellent agreement with the data. The positive matching of the force curves is mostly determined by the shape of the bows themselves which have already shown an excellent agreement with the simulation of Fig. 9a, b, and as reported in Supp. Mat. We can conclude that the discrepancy in the final force, which is directly proportional to the Young moduli of the materials and to the third power of the limb thickness, is attributed to the materials and errors in the geometry of the limb. The energy of the fully drawn bows, calculated as $\int^{0.65} F(b) db$, is 11.7 J, 13.5 J, and 14.5 J for the H1.5, H2.0, and H2.5 bows, respectively.



Fig. 11. Quantitative comparison between the measured stress (circles) and simulation (solid lines) of the target profile of the bows at full drawn calculated with the inverse model. The total stress σ_{tot} (red), σ_{bow} (blue), and pre-stress σ_{pre} (black) are measured for the three fabricated bows: (a) H1.5 bow, (b) H2.0 bow, and (c) H2.5 bow. The stress is measured on the surface of the glass fibre by using strain gauges. The total stress σ_{tot} is calculated as a sum of the stress of the target σ_{bow} and pre-stress of the material σ_{pre} .



Fig. 12. Quantitative comparison between the simulation and measurement of the stress σ_{bow} on the glass fibre laminate of the bows. σ_{bow} is simulated by using the direct model in (a), (c), and (e) whereas the measured stress is obtained from the 12 strain gauges attached to the surface of the glass fibre in (b), (d), and (f).

4.4. Stress measurements

The stress is the last parameter to confirm the inverse model and the non-curved beam approximation. We derive the stress distribution from the measured strain of the bow, by assuming a linear relationship $\sigma = E \cdot \epsilon$ between stress σ and strain ϵ , with E the Young modulus measured by the three-point bending test. Since the cross-section of the constructed bows is symmetric, we evaluate the strain of glass fibre on one side of the limb. To compare the stress of data and simulation we use the Young moduli of the glass fibre measured for each bow in Table 2. In the simulation, by using Eq. (16) for $q_t = c/2 + t$, we calculate the stress distribution of the target profile σ_{tot} on the surface of the glass fibre as a sum of pre-stress σ_{pre} and stress of

the bow σ_{bow} . In the same way, the experimental total stress is evaluated by summing the same quantities, calculated multiplying the Young modulus by the strain measured with strain gauges applied on the limbs.

Fig. 11 shows the comparison between the inverse model and measurement of σ_{pre} , σ_{bow} , and σ_{tot} . It should be noted that the simulation is not rescaled or normalized. The measured stresses in the three bows quantitatively show a good agreement with the distribution calculated by the inverse model. The RMSEs between the measured and computed points of the total stress σ_{tot} are 7.7 MPa, 7.0 MPa, and 5.7 MPa for the H1.5, H2.0, and H2.5 bows, respectively. The total stress of the bows increases as the curvature of the bow increases from the H1.5 to the H2.5 bow, due to the strain accumulated from the bow in its unbraced state to the full drawn state. The total stress of the glass fibre in the three bows is within 220 MPa, which is well within the limit of elastic deformation, as shown in Fig. 4a. On the one hand, the bow stress σ_{bow} is maximum at the centre of the bows, where the bending moment is maximum and decreases to zero at the limb's end, where the bending moment is zero ($m(L_i) = 0$). On the other hand, the pre-stress σ_{pre} in the laminates reduces the total stress at the grip ($s = 0$) and increases it at around $s_D \sim 0.2$ m and $s_U \sim 0.4$ m where the limbs are largely deformed.

To further validate the inverse model, we compare the bow stress σ_{bow} computed by using the direct model and the one measured by using the strain gauge and the drawing board. The stress is measured and calculated from a drawing length of $b = 15$ cm (slightly higher than the brace height of 13 cm) to the drawing length of the target at $b = 65$ cm. The complete mapping of the stress distribution as a function of the drawing and limb length of the bows is shown in Fig. 12. Again, it should be noted that the simulation and the data measured by using the strain gauge are not rescaled, and a quantitative comparison is shown. The stress distributions calculated by using the direct model in Fig. 12a, c, and e show a quantitatively good agreement with the measured stress in Fig. 12b, d, and f demonstrating the validity of the approximation of thin limb in the stress equation for the description of a largely deformed beam.

1. Conclusion

We demonstrated a systematic method for the design and manufacturing of FRP bows. The method is based on an inverse formulation of the elastica theory, in which the profile of the full drawn bow is used as the initial condition for the problem. The solutions of the model provided sufficient requirements for the construction of the bows with a determined shape and force. We validated our method by constructing three Japanese bows made of glass fibre and wood with different unbraced shapes and the same final force. We performed the bending test on glass fibre and various woods, and based on the criteria of the model, we evaluated the most suitable materials in terms of density, elastic stress, and ultimate stress. We showed that as a result of the large elastic deformation of glass fibre, the bows' dimensions, shape, and force could be precisely designed. We obtained an excellent agreement between the shape of the constructed bows with that predicted by the model, committing an error of a few millimeters, small as compared to the length of the bows of 1.62 m. In comparing the final force of the bows, we quantitatively committed an error within 5% with respect to the force of 5 kgf set by design, due to the variability of the materials. We compared the stress distribution on the bow's limbs, derived by the measurement of strain with strain gauges sensors, with that predicted by the model showing quantitatively accurate results. We committed an error in the order of a few MPa in predicting the stress distribution of glass fibre, which is small compared to the maximum stress measured in the three bows, in range of 170–220 MPa.

Compared with previous studies, our design method simplifies the problem of the limb deformation to the numerical resolution of a few equations, which could be implemented by bow-makers with the help of a spreadsheet. Our method finds application in the design of bows with a traditionally established shape. The use of a standardized shape simplifies the fabrication procedure of the bow and reduces the number of parameters for the optimization of the weight and dimensions of the limb. At the same time, the cultural heritage of a specific archery craftsmanship may be preserved by maintaining the characteristic profile of the fully drawn bow. With the advent of modern materials, our inverse model combined with FRP

composites allows a cost-effective solution for the manufacturing of traditional bows as sporting goods and competition archery equipment.

CRedit authorship contribution statement

Giacomo Mariani: Conceptualization, Methodology, Software, Investigation, Validation. **Eiichi Obataya:** Investigation, Resources. **Mahiro Kosaka:** Investigation. **Makinori Matsuo:** Supervision, Resources, Funding acquisition.

Declaration of competing interest

The authors declare that they have no known competing financial interests or personal relationships that could have appeared to influence the work reported in this paper.

Acknowledgements

This research was supported by the Kyudo specialized subcommittee in the Japanese Academy of Budo. The authors would like to thank Hiroumi Tsukuba from the Tsukuba Lumber Shop for providing the wood specimens tested in our laboratory. In addition, we thank Hunter Gott for proofreading the manuscript and Gaku Aizawa for the critical review of the manuscript.

Appendix A. Supplementary data

Supplementary material related to this article can be found online at <https://doi.org/10.1016/j.compstruct.2022.115722>.

References

- [1] [Bergman CA. The development of the bow in Western Europe: a technological and functional perspective. Archeol Pap Am Anthropol Assoc 1993;4\(1\):95–105.](#) [2] [Bergman CA, McEwen E. Sinew-reinforced and composite bows. In: Projectile technology. Springer; 1997, p. 143–60.](#) [3] [Grayson CE, French M, O'Brien MJ. Traditional archery from six continents: The Charles E. Grayson collection. University of Missouri Press; 2007.](#) [4] [Hickman CN. The dynamics of a bow and arrow. J Appl Phys 1937;8\(6\):404–9.](#) [5] [Hickman CN, Nagler F, Klopsteg PE. Archery: The technical side. National field archery association; 1947.](#) [6] [Kooi BW. The 'cut and try' method in the design of the bow. In: Eschenauer Hans A, Mattheck Claus, Olhoff Niels, editors. Engineering optimization in design processes. Berlin, Heidelberg: Springer Berlin Heidelberg; 1991, p. 283–92.](#) [7] [Kooi BW. The design of the bow. Proc Kon Ned Akad V Wetensch 1994;97\(3\):1–27.](#) [8] [Kooi BW, Bergman CA. An approach to the study of ancient archery using mathematical modelling. Antiquity 1997;71\(271\):124–34.](#)
- [9] Virk AS, Summerscales J, Hall W, Grove SM, Miles ME. Design, manufacture, mechanical testing and numerical modelling of an asymmetric composite crossbow limb. Composites B 2009;40(3):249–57. <http://dx.doi.org/10.1016/j.compositesb.2008.10.004>. [10] Demir S, Ekici B. Optimization of design parameters for Turkish Tirkeş (war) bow. Composites B 2014;66:147–55. <http://dx.doi.org/10.1016/j.compositesb.2014.04.029>. [11] [Moitinho de Almeida V, et al. Towards functional analysis of archaeological objects through reverse engineering processes. Universitat Autònoma de Barcelona; 2014.](#) [12] Hosoya S, Miyaji C, Kobayashi K. Computer simulation of restitution of Japanese bows. J Japan Soc Sports Ind 1995;5(2):25–33. <http://dx.doi.org/10.5997/j.sposun.5.2.25>. [13] Ohtsuki A, Ohshima S, Yamanaka S, Takeuchi H. Analysis of large deformation of Japanese bows. In: The proceedings of the computational mechanics conference, 2000.13. 2000, p. 61–2. <http://dx.doi.org/10.1299/jsmecmd.2000.13.61>. [14] Ohtsuki A, Ohshima S.

Nonlinear dynamic analysis of a Japanese bow (nonlinear spring characteristics and dynamic behavior). Trans Japan Soc Spring Eng 2019;2019(64):23–31. <http://dx.doi.org/10.5346/trbane.2019.23>.

[15] Mariani G, Matsuo M. The static deformation of the asymmetric Japanese bow: modelling bow asymmetries with the elastica theory. Meccanica 2020;55(9):1733–52. <http://dx.doi.org/10.1007/s11012-020-01213-2>. [16] Zenkert D. [An introduction to sandwich construction](#). Warley: EMAS Publ; 1995. [17] History of the Japanese FRP bow. Hiden Budo Bujutsu Mag 2012;23–33, URL <http://www.bab.co.jp/hiden/>. [18] URL <http://www.frpyumi.sakura.ne.jp/>. (visited on 2021/05/01). [19] URL <https://koyama-kyugu.co.jp/about/>. (visited on 2021/05/01). [20] Kooi BW. [On the mechanics of the bow and arrow](#). J Eng Math 1981;15(2):119–45. [21] Young WC, Budynas RG, Sadegh AM, et al. [Roark's formulas for stress and strain](#), Vol. 7. New York: McGraw-Hill; 2002. [22] Sanne M, Ahn-Ercan G, Pfriem A. [A mathematical solution for calculating the springback of laminated beech stacks molded within the elastic range](#). Forests 2020;11(7):725. [23] URL <https://www.smooth-on.com/products/ea-40/>. (visited on 2020/04/01).